PNAS
www.pnas.org

Supplementary Information for

Biased competition in the absence of input bias: insight from corticostriatal computation

Salva Ardid, Jason S. Sherfey, Michelle M. McCarthy, Joachim Hass, Benjamin R. Pittman-Polletta, Nancy Kopell

Corresponding Author: S. Ardid.
E-mail: sardid@bu.edu

This PDF file includes:

www.pnas.org/cgi/doi/10.1073/pnas.1812535116

Supplementary Text

There are two points we focus on in this supplementary section. First, we describe the foundations upon which we implemented our striatal circuit model. Second, we describe how mechanisms other than the coherence bias mechanism, fail to be consistent with observed rhythmic activity in PFC in the context of rule-based decisions.

Building a striatal circuit model of preferential processing

Our striatal circuit model builds upon previous work (1). Our current implementation differs, however, from the previous model in four relevant aspects:

Two spiny projection neuron phenotypes. This version of the model considers the two main phenotypes of spiny projection neurons (SPNs): D1 and D2 SPNs. SPNs together constitute about 95% of the cells in the striatum and, unlike other cell types in the striatum, these cells receive the majority of inputs and are the only cells projection downstream to other nuclei of the basal ganglia (2).

D1 and D2 SPNs possess an asymmetric connectivity profile (3) (Fig. 2A). To analyze how the asymmetric, sparse connectivity affects circuit dynamics, we compared the control population-averaged f-I curves (Fig. 3C) with the same f-I curves assuming all-to-all connectivity (Fig. S1). The comparison of f-I curves reveals that no substantial difference is found if the maximal conductance is rescaled by the connectivity ratio. Thus, the main role of asymmetric connectivity in circuit dynamics is to modulate the GABAergic directionality between D1 and D2 SPNs.

Health condition. Our model aims to represent the dynamics of SPNs in health condition, whereas the previous model was a striatal model of Parkinson's Disease (PD), which assumed dopamine depletion. The overall increase in dopamine concentration in health compared to *in vitro* recordings or PD (4, 5) affects the intrinsic excitability of each SPN phenotype in opposite directions (6): while D2 SPNs excitability strongly decreases, D1 SPNs excitability increases, up to a point where no apparent differences exist between the baseline activity of D1 and D2 SPNs (7).

Dopamine concentration ([DA]) also impacts neural dynamics at the circuit level via neuromodulation of GABAergic synapses (8) (Fig. 2B). In our model, we considered these high vs. low [DA] *in vitro* recordings as a proxy for [DA] in health and PD, respectively. We therefore adjusted the parameters of GABA synapses in our model to be consistent with the experimental observation at high [DA], maintaining the maximal conductance ratio between D1 and D2 SPNs, and fitting the relaxation time of depression, individually for D1 and D2 SPNs (Fig. 2B).

Calcium dynamics. Our current version of the model accounts for the stronger activation of calcium-dependent potassium channels in D2 SPNs compared to D1 SPNs, reported experimentally (9) (Fig. 2C). This is mediated by a higher maximal conductance of the inward high-threshold calcium current in D2 SPNs.

SPNs resonance. Beta oscillations in the previous version of the model emerged from a rebound mechanism originated from an interaction between the intrinsic outward M-type potassium current and the network GABAergic synaptic inputs (1). In contrast, in this version of the model, SPN beta resonances (Fig. 3E) emerge from excitatory inputs and rely purely on the network GABAergic synaptic mechanism, as inferred from strengthened beta resonances following the absence of M-type input currents (Fig. S2 vs. Fig. 3E low input panel).

Diversity of interneurons in the striatum

We acknowledge the large diversity and relevance of interneurons in the striatum (10). For instance, fast-spiking interneurons do not only mediate feedforward inhibition but also regulate synaptic plasticity (11)). The impact of the diverse set of striatal interneurons on actively gating rule-based decisions is, however, far from understood. At this point, we lack sufficient experimental constraints to build and guide a more comprehensive computational model, in which functional hypotheses can materialize in mechanistic predictions of how these cell types orchestrate rule-based decisions. In our opinion, future studies should focus on how cortical inputs and striatal interneurons dynamically shape corticostriatal selectivity for action selection, in particular through different phases of learning.

Comparison between our model and (12)

The main difference between our model and (12) is in the shapes of the f-I curves for D1 and D2 SPNs in health condition (Fig. 3C compared to Fig. 1B in (12)), which results in opposite turning transitions of overall excitability between D1 and D2 SPNs. This difference in dynamics between the two models is (presumably) explained by the following underlying mechanisms:

- In contrast to our model, (12) considers fast-spiking interneurons (FSIs), which mediate stronger feedforward inhibition to D1 SPNs. To overcome the higher excitability of D2 SPNs, Bahuguna and colleagues added stronger cortical inputs targeting D1 SPNs, either via increased presynaptic firing rate or by means of stronger cortical synapses. Note, however, that the compensation of higher overall excitability of D2 SPNs is only effective for low FRs (up to a threshold of 13 sp/s, given the set of parameters in (12)).

- On the other hand, (12) did not consider other physiological differences between SPNs. In particular, we show in our study that distinct properties in GABAergic short-term depression and in calcium-dependent potassium currents between SPNs are relevant (Figs. 2B and 2C).

Models are based on assumptions, so the question is whether those assumptions are well suited. The answer to this question certainly depends on the specifics of the study. In our model, we omitted FSIs under the assumption that they spread out a blanket of feedforward inhibition, whose principal function is to silence the activity of non-relevant SPNs (13), i.e., those SPNs that are not directly involved in action selection for the particular cortical input at hand.

Importantly, recent experimental evidence (14) shows that FSIs, preferentially targeting D1 SPNs, are: (i) principally distributed topographically in the dorsolateral striatum, (ii) associated with habitual behavior, (iii) strongly gamma rhythmic, which could help to understand why the activation of FSIs (iv) selectively enhances the firing rate of D1 SPN ensembles. Our study instead focuses on the (dorsomedial) striatal circuit mediating goal-directed behavior. In this scenario, the role of FSIs and their gamma entraintment are de-emphasized (14), which is in line with our assumptions, but challenges the approach in (12) to account for rule-based decisions and the suggested role of alpha and beta rhythms in the pfc in this context (15).

Another difference between the two models focuses on cortical inputs of low strength that favor D1 SPNs (GO) in (12), in contrast to D2 SPNs (NO-GO) in our model, which we propose might be behaviorally advantageous. Consequently, the direction of the bias in (12) does not fit with the NO-GO pathway prevalence for inputs of high uncertainty (i.e., inputs of low signal-to-noise ratio).

In summary, the two models predict an opposite turning transition in overall excitability between D1 and D2 SPNs. Experimental testing should identify which of the two models better represents the striatal circuit in health condition. But, the experimental answer to this question may likely depend on the type of task (goal-directed vs. habitual behavior), the striatal region under study (dorsomedial vs. dorsolateral), and whether or not learning is involved, and if so, the learning stage at which the prediction is checked.

Mean-field approximation

Even though a mean-field implementation of this model is out of the scope of this study, we think that a rate version of the model will likely reproduce the different regimes of excitability shown in the f-I curves (Fig. 3C and Fig. S1), under the assumption that such a model fully accounts for network (GABA input) and intrinsic (Ca^{2+} dependent currents) dynamics (as shown in Fig. 2B and 2C, respectively). See (16) for a similar approach in terms of NMDA dynamics.

Whether this type of mean-field approach will also be able to replicate the striatal resonances describing the synchrony among neurons within a ensemble (Fig. 3E) is less obvious. Nevertheless, we believe that this might be the case because the mechanism supporting resonant dynamics in our model purely relies on recurrent GABAergic inputs between SPNs. Thus, a rate model endowed with GABAergic dynamics and built so that the rate dynamics describes the instantaneous firing rate of each neuronal ensemble, as in our model, might be a candidate mean-field model to reproduce our results.

Internal biased competition mechanisms not consistent with reported rule-based rhythmic activity

According to (15), modulated high beta oscillatory activity in PFC is associated with rule-based action selection, presumably mediated by preferential activation of relevant D1 SPNs (relevant GO pathway) vs. irrelevant D1 SPNs (irrelevant GO pathway) and D2 SPNs (NO-GO pathway), whereas alpha oscillatory activity in PFC is associated with inhibitory control, presumably mediated by preferential activation of D2 SPNs (NO-GO pathway) against D1 SPNs (GO pathway). Such a picture is not fully consistent with the following two internal biased competition mechanisms:

Rate bias mechanism. Only the slow integrator decoder is able to specifically read out rate biases. Thus,

- For high beta inputs, we limit the analysis to compare the activity of relevant vs. irrelevant D1 SPNs for high input strength only, because this is the condition in which D1 SPN activity (GO pathway) surpasses the activity of D2 SPNs (NO-GO pathway) (Fig. 3C). As seen in Figure 5A bottom, the slow integrator decoder is unable to reliably distinguish the activity of relevant and irrelevant D1 SPNs, hence it is incapable of responding according to the relevant feature of the stimulus. This is in contrast to the fast integrator decoder, which naturally reads out the coherence bias (Fig. 5A).

- For alpha inputs, we limit the analysis to the low strength input, because this is the only condition in which D2 SPN activity surpasses the activity of D1 SPNs (Fig 3C). Even though the slow integrator decoder is able to respond according to the activity of D2 SPNs (Fig. S3A slow integrator panel), this is not due to the spectral content of the input, as it was the case in (Fig. 5B). Instead, it is mediated by the low strength of the input (see Fig. 4A bottom). This is confirmed by analogous dynamics under high beta oscillatory inputs (Fig. S3B slow integrator panels).

Coexisting biases. The coexistence bias mechanism assumes the low strength input and a shift in the regime of operation of the read-out decoder (Fig. 4C), so that the decoder is able to respond either to the overall higher firing rate of D2 SPNs (slow integrator decoder), or to the higher coherence bias of D1 SPNs (fast integrator decoder). Thus,

- The case of alpha inputs is the same here as in the rate bias mechanism. The slow integrator decoder indeed preferentially processes D2 SPNs activity bias, but this is not specific to a rhythmic input in the alpha frequency band (Fig. S3 slow integrator panels).

- The dynamics under the high beta oscillatory input of low strength is more difficult to predict, given the mismatch between the frequency of the cortical input at high beta frequency and SPNs resonance at lower beta frequency (Fig. 3E low input panel). Are relevant D1 SPNs able to transform a high beta coherence bias in PFC input into a coherence output bias with respect to irrelevant D1 SPNs and D2 SPNs? Figure S3B (fast integrator panels) shows that this is actually not the case: even though relevant D1 SPNs are more strongly synchronized than irrelevant D1 SPNs (Fig. S3B left vs. right fast integrator panels), D2 SPNs become synchronized more rapidly than D1 SPNs (Fig. S3B fast integrator panels), and even later on, D1 and D2 SPNs become similarly synchronized (Fig. S3B fast integrator panels).

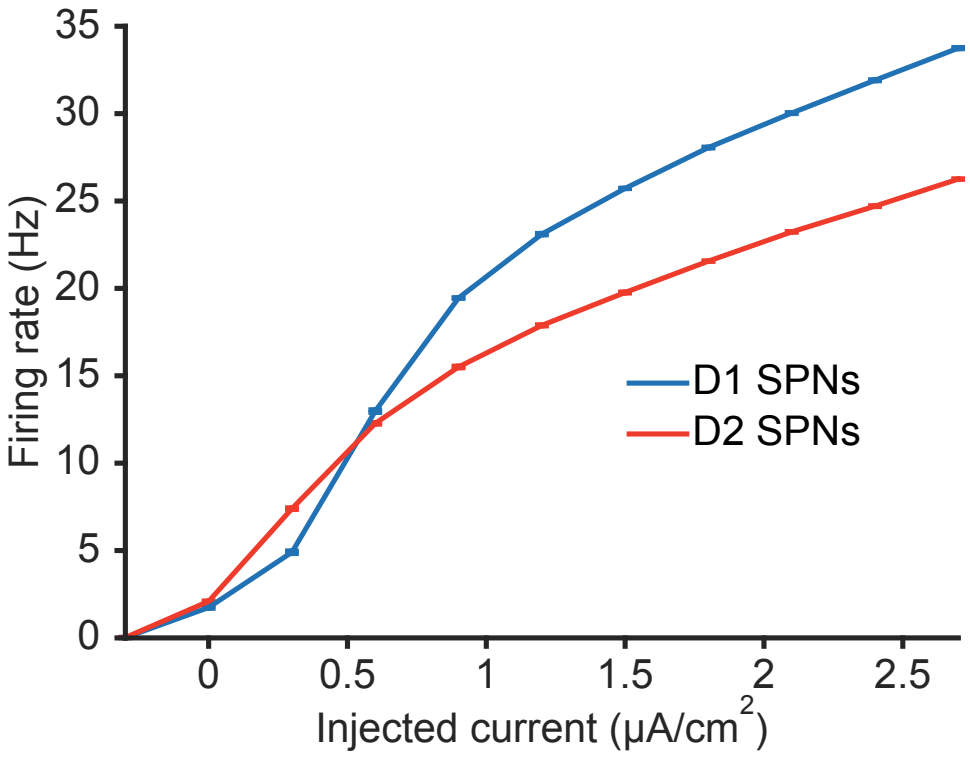

Fig. S1

Fig. S1. Averaged f-I curve of D1 and D2 SPNs under all-to-all connectivity. The curves represent the input-output relationship between injected current and time-averaged population firing rate under all-to-all connectivity. For this analysis, GABAergic conductances have been scaled down by the reported connectivity ratio (3), so that the effective conductance stays the same with respect to the conductance under asymmetric, sparse connectivity.

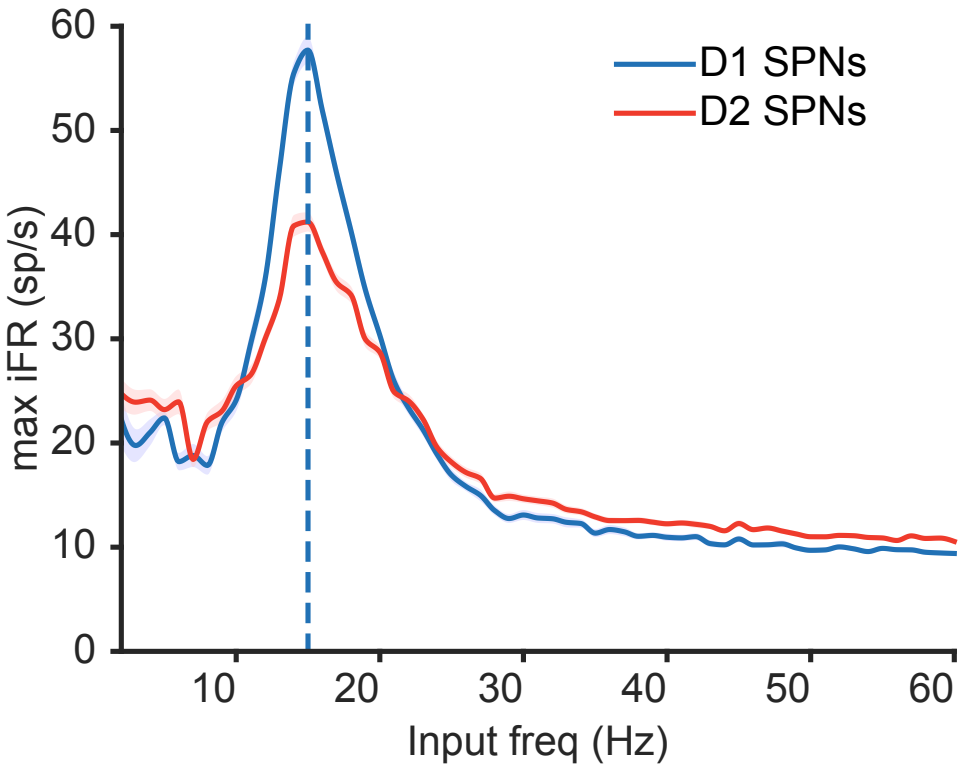

Fig. S2

Fig. S2. Resonance of SPNs for the low strength input in the absence of M-type input currents. The resonance is quantified in terms of maximum iFR, a measure of local population synchronization: across input frequencies (x-axis), the average of the peak iFR through all cycles is computed (y-axis).

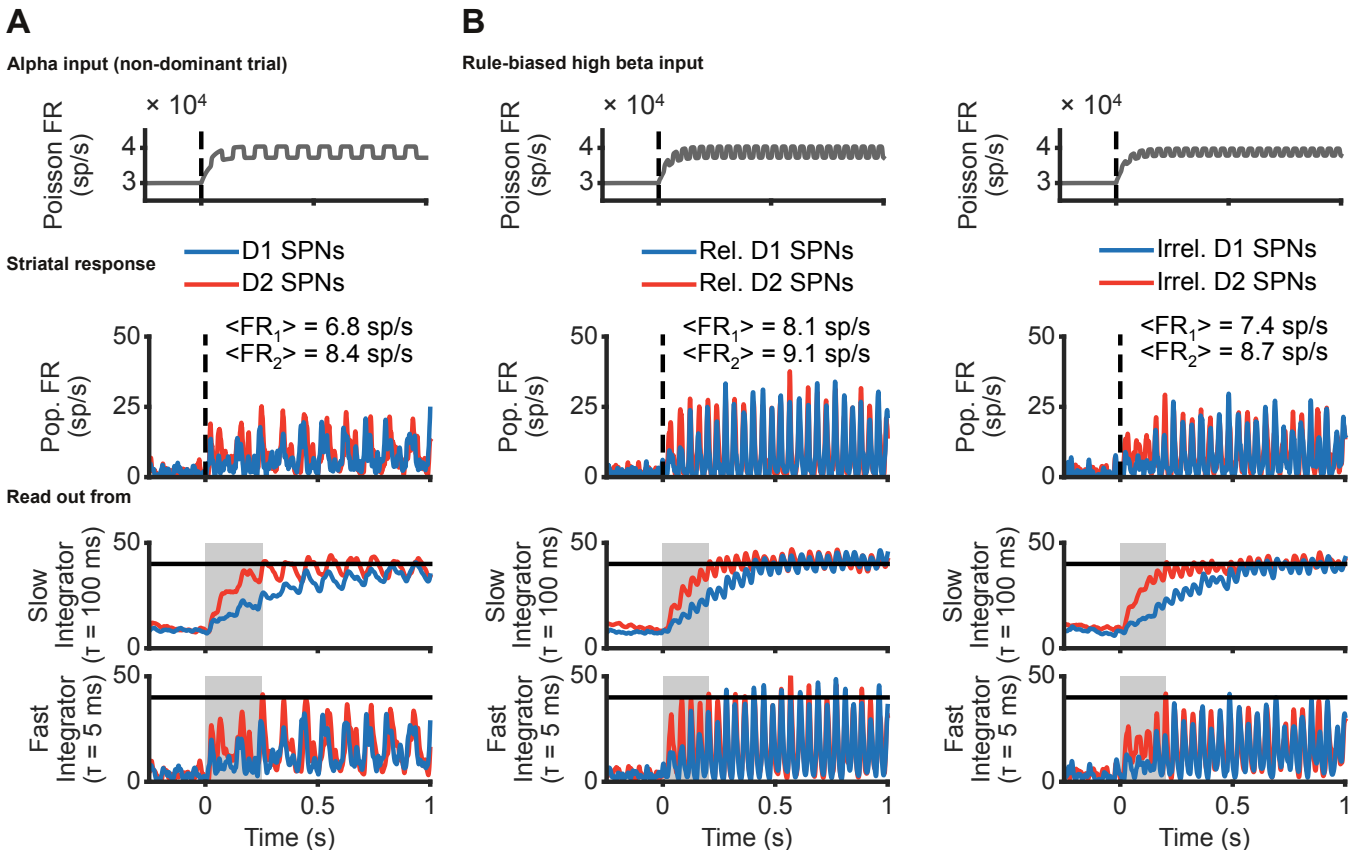

Fig. S3

Fig. S3. Striatal processing of the low strength input oscillating at alpha and high beta frequencies. (**A**) Alpha input. Top: Low strength, alpha rhythmic input. Middle: Population FR varying in time (iFR). Bottom: Downstream readout of the activity of SPNs using distinct integration timescale. Response time is shaded in light gray. Response threshold at 40 sp/s (solid horizontal line). (**B**) Rule-biased high beta inputs (see main and supplementary text for details). Top: Relevant SPNs (left) receive more synchronized inputs (oscillations of higher amplitude) compared to irrelevant SPNs (right). Middle: Population FR varying in time (iFR). Bottom: Downstream readout of the activity of SPNs using distinct integration timescale. Response time is shaded in light gray. Response threshold at 40 sp/s (solid horizontal line).

Supplementary Materials and Methods

Model specification

Our striatal model consists of two populations of neurons, each population ($N = 150$) representing a distinct type of spiny projection neurons (SPNs) according to dopamine receptor expression: D1R vs. D2R. Each SPN is modeled by a single compartment, representative of the soma. The membrane voltage V (mV) of each cell integrates input currents in time according to the following first order ordinary differential equation (ODE):

$$C_m \frac{dV}{dt} = -\sum I_x(t, V)$$

where t refers to time (ms), C_m is the membrane capacitance ($1\mu\text{F/cm}^2$), and I_x ($\mu\text{A/cm}^2$) spans three distinct input types: I_{intr} for intrinsic input from ionic channels, $I_{syn,int}$ for synaptic inputs from striatal SPNs, and $I_{syn,ext}$ for synaptic inputs from external sources.

Intrinsic input currents. I_{intr} consists of inward fast sodium I_{Na}, outward fast delayed rectifier potassium I_K, leak I_L, outward M-type potassium I_M, inward high-threshold calcium I_{Ca}, and outward calcium-dependent potassium I_{KCa} components. I_{Na}, I_K, I_L, I_M, and I_{Ca} are modeled following the Hodgkin-Huxley formulation:

$$I = g \cdot m^n(t, V) h^k(t, V)[V - E]$$

where g denotes the maximal conductance (mS/cm^2), E is the reversal potential (mV), and $m(t, V)$ and $h(t, V)$ represent activation and inactivation gating variables of n and k order kinetics ($n, k \geq 0$), respectively.
Ion channel gating variables, x in {m,h}, are described in time by a two-state kinetic first order ODE. They can be either expressed in terms of opening and closing channel rates, $\alpha_x(V)$ and $\beta_x(V)$, as follows

$$\frac{dx}{dt} = \alpha_x(V)[1 - x] - \beta_x(V)x$$

or in terms of the steady-state and the time constant, $x_\infty(V)$ and $\tau_x(V)$

$$\tau_x(V) \frac{dx}{dt} = x_\infty(V) - x$$

according to the relationship of x_∞ and τ_x with respect to α_x and β_x:

$$x_\infty(V) = \alpha_x(V)/[\alpha_x(V) + \beta_x(v)] \qquad \tau_x(V) = 1/[\alpha_x(V) + \beta_x(V)]$$

For the I_{Na} current, $g_{Na} = 100mS/cm^2$, $E_{Na} = 50mV$, $n_{Na} = 3$ and $k_{Na} = 1$. The rate functions (α_{Na} and β_{Na}) for the activation (m_{Na}) and inactivation (h_{Na}) gating variables are:

$$\alpha_{m,Na}(V) = \frac{0.32(V+54)}{1-exp[-(V+54)/4]} \qquad \alpha_{h,Na}(V) = 0.128exp[-(V + 50)/18]$$

$$\beta_{m,Na}(V) = \frac{-0.28(V+27)}{1-exp[(V+27)/5]} \qquad \beta_{h,Na}(V) = \frac{4}{1+exp[-(V+27)/5]}$$

For the I_K current, $g_K = 80mS/cm^2$, $E_K = -100mV$, $n_K = 4$ and $k_K = 0$ (i.e., no inactivation). The rate functions (α_K and β_K) for the activation (m_K) gating variable are:

$$\alpha_{m,K}(V) = \frac{0.032(V+52)}{1-exp[-(V+52)/5]} \qquad \beta_{m,K}(V) = 0.5exp[-(V + 57)/40]$$

For the I_L current, $E_K = -67mV$, $n_K = 0$ and $k_K = 0$ (i.e., no gating variables). g_L is slightly different between D1 and D2 SPNs: $0.097mS/cm^2$ and $0.1mS/cm^2$ respectively, which accounts for non-significantly different baseline activities between the two phenotypes (7).
For the I_M current, $g_M = 1.3mS/cm^2$, $E_M = -100mV$, $n_M = 1$ and $k_M = 0$ (i.e., no inactivation). The rate functions (α_M and β_M) for the activation (m_M) gating variable are:

$$\alpha_{m,M}(V) = \frac{3.209 \cdot 10^{-4}(V+30)}{1-exp[-(V+30)/9]} \qquad \beta_{m,M}(V) = \frac{-3.209 \cdot 10^{-4}(V+30)}{1-exp[(V+30)/9]}$$

For the I_{Ca} current, $E_{Ca} = 120mV$, $n_{Ca} = 2$ and $k_{Ca} = 0$ (i.e., no inactivation). g_{Ca} is different between D1 and D2 SPNs: $0.018mS/cm^2$ and $0.025mS/cm^2$ respectively, which accounts for faster and stronger activation of the I_{KCa} current in D2 SPNs (9)(Fig. 2C). The rate functions (α_{Ca} and β_{Ca}) for the activation (m_{Ca}) gating variable are:

$$\alpha_{m,Ca}(V) = \frac{1.6}{1+exp[-(V-65)/13.889]} \qquad \beta_{m,Ca}(V) = \frac{-0.02(V-51.1)}{1-exp[(V-51.1)/5]}$$

For the I_{KCa}, $g_{KCa} = 0.2mS/cm^2$ and $E_{KCa} = -80mV$. I_{KCa}, however, activates by calcium concentration (in mM) instead of voltage ($n_{KCa} = 1$ and $k_{KCa} = 0$, i.e., no inactivation). For simplicity, the time constant of activation is considered fixed at $\tau_{m,KCa}([Ca]) = 120ms$, whereas the steady-state of the activation (m_{KCa}) gating variable is:

$$m_{\infty,KCa}([Ca]) = \frac{1}{1 + exp[-([Ca] - 0.075)/0.01]}$$

$[Ca]$ varies according to the following calcium buffer dynamics

$$\frac{d[Ca]}{dt} = f_{[Ca]} I_{Ca} - [Ca]/\tau_{[Ca]}$$

where $f_{[Ca]} = 18 \frac{mM/ms}{\mu A/cm^2}$ is the $[Ca]$ accumulation factor and $\tau_{[Ca]} = 50ms$ represents the decay time in calcium concentration.

Synaptic input currents among SPNs. $I_{syn,int}$ refers to the inhibitory synaptic inputs between striatal SPNs mediated by GABAA receptors. For each SPN, $I_{syn,int}$ is modeled according to:

$$I_{syn,int} = \sum_{i}^{N_{pre}} g_{GABAA} \cdot s_i(t,V)[V - E_{GABAA}]$$

where $E_{GABAA} = -80mV$ represents the reversal potential and g_{GABAA} refers to the maximal gabaergic conductance, whose value ($0.65mS/cm^2$) is divisively normalized by the number of presynaptic cells of each phenotype ($N_{pre} = 150$) and multiplicatively scaled by up to three factors. The first factor (0.635) applies specifically to presynaptic D2 SPNs to adjust for a higher first postsynaptic current emerging from D1 SPNs at high [DA] levels (8) (Fig. 2B). The second factor determines the number of synaptic contacts between SPN phenotypes, which is randomly sampled according to the different proportion of synaptic connections (3) (Fig. 2A): 0.26 from D1 to D1 SPNs, 0.06 from D1 to D2 SPNs, 0.27 from D2 to D1 SPNs, 0.36 from D2 to D2 SPNs. The third factor (1.5) qualitatively accounts for stronger cross-inhibition (between D1 and D2 SPNs) compared to self-inhibition (within D1 and D2 SPNs) (3).
$s_i(t,V)$ represents presynaptic gating variables, whose dynamics evolves according to the following first order ODE:

$$\frac{ds_i}{dt} = -s_i/\tau_s + 2[1 + tanh(V/4)](1 - s_i)D_i$$

where the decay time of inhibition, τ_s, is sampled from a normal distribution centered at $30.4ms$ with a standard deviation of $8.2ms$ to be in agreement with (8). $D_i(t,V)$ accounts for presynaptic short-term depression between SPN synapses:

$$\frac{dD_i}{dt} = (1 - D_i)/\tau_D - \alpha_D[1 + tanh(V/4)](1 - \delta_D)D_i$$

where $\alpha_D = 2.305$ and $\delta_D = 0.35$ control how much depression is accumulated after each spike, and τ_D is the decay time of depression, which is significantly longer in D1 SPNs ($1030ms$) than in D2 SPNs ($210ms$). These parameters were adjusted according to (8)(Fig. 2B).

External synaptic input currents. $I_{syn,ext}$ refers to the long-range excitatory synaptic inputs to striatal SPNs from external sources, which are modeled according to stochastic Poisson spike trains. $I_{syn,ext}$ accounts for two distinct components: the background input, an asynchronous, uncorrelated, and unspecific input, whose strength determines the baseline activity of SPNs; and a task-dependent cortical input, assumed to be equal for D1 and D2 SPNs (17). For simplicity, both components are assumed to be mediated by AMPA receptors. Thus, for each SPN, $I_{syn,ext}$ is modeled according to:

$$I_{syn,ext} = g_{bkg} \cdot s_{bkg}(t)[V - E_{AMPA}] + g_{ctx} \cdot s_{ctx}(t)[V - E_{AMPA}]$$

where $E_{AMPA} = 0mV$ represents the reversal potential. The maximal AMPA conductance is set to $g_x = 3.5\mu S/cm^2$ for both components x in {bkg, ctx}. $s_x(t)$ represents the gating variables, modeled as instantaneous jumps of magnitude 1 for each presynaptic spike followed by an exponential decay of $\tau_s = 2ms$. The two components differ, however, in terms of the Poisson process representing presynaptic firing.
For the background input, each SPN in each simulation is targeted by a different realization of a homogeneous Poisson process representing a total presynaptic firing of $r_{bkg} = 30kHz$, which can be mediated, for instance, by 15 thousand synapses (18) transmitting $2sp/s$ on average.
In contrast, the properties of the task-dependent cortical input differs in distinct simulations: the cortical input may be asynchronous (homogeneous Poisson process) or rhythmic (inhomogeneous Poisson process), it may be of higher or lower overall strength, and, if rhythmic, the input may oscillate at distinct frequency bands. To avoid sudden transitions at stimulus onset, the cortical input ramps up exponentially with a time constant of $\tau_{ctx} = 40ms$.
Specifically, the asynchronous input of high strength is mediated by a stochastic Poisson process representing a total presynaptic firing of $r_{ctx}^{DC,high} = 44kHz$. For high strength inputs, the amplitude of the rhythmic modulation is $r_{ctx}^{AC,high} = 8kHz$. The low strength input scales down these values 5 times to $r_{ctx}^{DC,low} = 8.8kHz$ and $r_{ctx}^{AC,low} = 1.6kHz$. Figure 3E shows the resonance of SPNs under distinct scaling factors: 0.2 (low strength input condition), 0.3, 0.4, 0.5, 0.6, and 1 (i.e., high strength input condition).
In the context of rule-based decisions, the rhythmic modulation of the input to SPNs encoding the irrelevant features is scaled down 1.6 times, with respect to SPNs encoding the relevant features (Fig. 5A and S3B), to account for the diminished synchrony of those neuronal ensembles in prefrontal cortex (15).
The frequency of the rhythmic, hence inhomogeneous, Poisson process is either centered at alpha frequencies $f_c = 10Hz$, or at distinct beta bands: $f_c = 18Hz$ targets the resonance of both SPN types at low input strength, whereas $f_c = 25Hz$ and $f_c = 20Hz$ target, at high input strength, the resonance of D1 and D2 SPNs, respectively. All these frequencies represent the

center around which the instantaneous frequency of each cycle jitters. In other words, the period of the oscillation slightly varies from cycle to cycle.
Cortical coordination is modeled as a smoothed square signal, arguably a better proxy of rhythmic synchronization in cortex compared to a sinusoid. The particular signal is implemented using periodic sigmoidal functions, of $1ms$ slope to generate smooth but sharp up and down transitions.

Data analysis

Population activity. Spiking multi-unit activity (MUA) is pooled over cells, separately for D1 and D2 SPNs ($N = 150$). The instantaneous firing rate is then estimated from MUA as follows: first, MUA is re-sampled from $\Delta t = 0.05ms$ to $\Delta t = 1ms$, after which, the Nadaraya-Watson smoothing kernel regression algorithm is applied with a $5ms$-bandwidth Epanechnikov kernel density estimator.

Read-out decoders. To quantitatively test if biases in striatal activity suffice to trigger robust downstream action selection, we devised a simple, yet quantitative, approach based on read-out decoders. Specifically, the read-out of striatal output is estimated using two alternative decoders that accumulate SPNs activity at distinct pace (fast vs. slow integrator), but that are otherwise identical. The instantaneous firing rate output of the read-out decoder r_{dec} evolves in time according to the following first order ODE:

$$\frac{dr_{dec}}{dt} = -\frac{r_{dec}}{\tau_{dec}} + k \cdot r_x$$

where τ_{dec} is either $5ms$ or $100ms$, respectively for the fast and slow integrator. r_x represents the striatal output, i.e., SPNs instantaneous firing rate, where x is a label either referring to D1 or D2 SPNs. k is a scaling factor (in s^{-1}) that is adjusted on a simulation basis so that the two read-out decoders are able to reach the same fixed response threshold at $40sp/s$. k_{slow} and k_{fast} are set to $\{46, 15.25, 40, 14.7, 14.7, 14.7, 14.2, 45, 45, 46\}$ and $\{480, 150, 200, 110, 110, 110, 122, 390, 380, 380\}$ respectively, for the following ten conditions: low strength asynchronous input (Fig. 4A), high strength asynchronous input (Fig. 4B), low strength input oscillating at SPNs resonance (Fig. 4C), high strength input oscillating at D1 SPNs resonance (Fig. 4D), high strength input oscillating at D2 SPNs resonance (Fig. 4E), rule-biased high beta input of high strength (Fig. 5A), alpha input of high strength (Fig. 5B), alpha input of low strength (Fig. S3A) and rule-biased high beta input of low strength, for relevant (Fig. S3B left) and irrelevant (Fig. S3B right) SPNs.

Implementation

The model was implemented in DynaSim (19), an open-source toolbox for simulating dynamical systems, compatible with MATLAB and GNU Octave. Simulations were executed using the fourth-order Runge–Kutta integration algorithm with a time step of $\Delta t = 0.05ms$. Simulations for the conditions shown in Results were executed using five different random seeds. No qualitative differences were found among distinct realizations, indicative of the robustness of the model against the two sources of randomness in the model: the stochastic Poisson processes underlying external inputs to the striatal circuit, and the randomly sampled sparse connectivity between SPNs. The output of the read-out decoders was integrated with the variable time step *ode*45 built-in ODE solver in MATLAB/GNU Octave, which implements the fourth-order Dormand-Prince integration method.

References

1. McCarthy MM, et al. (2011) Striatal origin of the pathologic beta oscillations in Parkinson's disease. *Proc. Natl. Acad. Sci. U.S.A.* 108(28):11620–11625.
2. Gerfen C, Bolam J (2017) The neuroanatomical organization of the basal ganglia in *Handbook of Basal Ganglia Structure and Function.* (Elsevier) Vol. 24, pp. 3–32.
3. Taverna S, Ilijic E, Surmeier DJ (2008) Recurrent collateral connections of striatal medium spiny neurons are disrupted in models of Parkinson's disease. *J Neurosci* 28(21):5504–5512.
4. Albin RL, Young AB, Penney JB (1989) The functional anatomy of basal ganglia disorders. *Trends Neurosci.* 12(10):366–375.
5. DeLong MR (1990) Primate models of movement disorders of basal ganglia origin. *Trends Neurosci.* 13(7):281–285.
6. Gerfen CR, Surmeier DJ (2011) Modulation of striatal projection systems by dopamine. *Annu Rev Neurosci* 34:441–466.
7. Parker JG, et al. (2018) Diametric neural ensemble dynamics in parkinsonian and dyskinetic states. *Nature.*
8. Tecuapetla F, Carrillo-Reid L, Bargas J, Galarraga E (2007) Dopaminergic modulation of short-term synaptic plasticity at striatal inhibitory synapses. *Proc Natl Acad Sci USA* 104(24):10258–10263.
9. Arias-Garcia MA, et al. (2013) Duration differences of corticostriatal responses in striatal projection neurons depend on calcium activated potassium currents. *Front Syst Neurosci* 7:63.
10. Tepper JM, et al. (2018) Heterogeneity and Diversity of Striatal GABAergic Interneurons: Update 2018. *Front Neuroanat* 12:91.
11. Owen SF, Berke JD, Kreitzer AC (2018) Fast-Spiking Interneurons Supply Feedforward Control of Bursting, Calcium, and Plasticity for Efficient Learning. *Cell* 172(4):683–695.

12. Bahuguna J, Aertsen A, Kumar A (2015) Existence and control of Go/No-Go decision transition threshold in the striatum. *PLoS Comput. Biol.* 11(4):e1004233.
13. Mallet N, Le Moine C, Charpier S, Gonon F (2005) Feedforward inhibition of projection neurons by fast-spiking GABA interneurons in the rat striatum in vivo. *J. Neurosci.* 25(15):3857–3869.
14. O'Hare JK, et al. (2017) Striatal fast-spiking interneurons selectively modulate circuit output and are required for habitual behavior. *Elife* 6.
15. Buschman TJ, Denovellis EL, Diogo C, Bullock D, Miller EK (2012) Synchronous oscillatory neural ensembles for rules in the prefrontal cortex. *Neuron* 76(4):838–846.
16. Wong KF, Wang XJ (2006) A recurrent network mechanism of time integration in perceptual decisions. *J. Neurosci.* 26(4):1314–1328.
17. Ballion B, Mallet N, Bezard E, Lanciego JL, Gonon F (2008) Intratelencephalic corticostriatal neurons equally excite striatonigral and striatopallidal neurons and their discharge activity is selectively reduced in experimental parkinsonism. *Eur J Neurosci* 27(9):2313–2321.
18. Oprisan SA, Buhusi CV (2014) What is all the noise about in interval timing? *Philos. Trans. R. Soc. Lond., B, Biol. Sci.* 369(1637):20120459.
19. Sherfey JS, et al. (2018) DynaSim: A MATLAB Toolbox for Neural Modeling and Simulation. *Front Neuroinform* 12:10.